Computer Physics Communications 308 (2025) 109438

Contents lists available at ScienceDirect

Computer Physics Communications

journal homepage: www.elsevier.com/locate/cpc

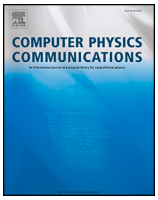

Computational Physics

Multiresolution of the one dimensional free-particle propagator. Part 2: Implementation☆

Evgueni Dinvay

Department of Chemistry, UiT The Arctic University of Norway, PO Box 6050 Langnes, N-9037 Tromsø, Norway

A B S T R A C T

A novel method to integrate the time-dependent Schrödinger equation within the framework of multiresolution analysis is presented. The method is based on symplectic splitting algorithms to separate the kinetic and potential parts of the corresponding propagator. The semigroup associated with the free-particle Schrödinger operator is represented in a multiwavelet basis. The propagator is effectively discretised with a contour deformation technique, which overcomes the challenges presented by previous discretisation methods. The discretised operator is then employed in simple numerical simulations to test the validity of the implementation and to benchmark its precision.

1. Motivation

This paper is devoted to temporal discretisation of the Schrödinger type equation

$$i\partial_t u = -\partial_x^2 u + V(x,t)u. \tag{1.1}$$

Combined together with the spatial discretisation considered in [11], it constitutes a complete numerical treatment of Equation (1.1) in the multiresolution analysis (MRA) framework.

We remind that in [11] a thorough description of the semigroup $\exp\left(it\partial_x^2\right)$ in multiwavelet bases was given. This exponential is a propagation operator associated with the free-particle Schrödinger equation

$$i\partial_t u + \partial_x^2 u = 0. \tag{1.2}$$

As we pointed out in [11], our multiwavelet representation of the semigroup $\exp\left(it\partial_x^2\right)$ can be considered sparse, provided that the time parameter t is big enough. This in turn limits the range of possible temporal schemes one can use for numerical simulation of (1.1). With the mentioned t-size restriction in mind, we make an extended review on high-order symplectic integrators in Section 2, advocating for those containing the biggest possible time parameters in their kinetic energy exponentials. One of the simplest second-order symplectic splitting methods can be introduced through the following factorisation

$$e^{At+Bt} = e^{Bt/2}e^{At}e^{Bt/2} + \mathscr{O}\left(t^3\right), \tag{1.3}$$

with $A = i\partial_x^2$ and $B = -iV$ in relation to Equation (1.1). Though the validity of the asymptotic factorisation (1.3) holds true for small t, we shall see below that the use of such times can be still considered acceptable when it comes to spatial multiwavelet representation. In other words, we argue that by carefully choosing a proper symplectic integrator one can respect both restrictions: the t-smallness accounting for validity of exponential factorisation and the t-bigness necessary for sparsity of the semigroup multiresolution.

The paper is organised as follows. We gather all the necessary information about high-order symplectic integrators in Section 2. Our numerical multiwavelet representation of $\exp\left(it\partial_x^2\right)$ is tested by running numerical simulations for toy benchmark models in Section 3. A summary of the first part [11] and of the current contribution is provided in Section 4 with some plans for future works.

2. Introduction to exponential integrators

It is known that a fundamental solution of the general linear equation

$$\partial_t u = Au + Bu \tag{2.1}$$

forms a two-parameter family of operators $\mathscr{T}(t_2,t_1)$ called propagator. It means that for any solution $u = u(t)$ of (2.1) and time moments t_1, t_2 we have $u(t_2) = \mathscr{T}(t_2,t_1)u(t_1)$. This section serves as a brief summary of how this propagator can be approximated by the exponential operators e^{At}, e^{Bt}, providing us with effective numerical schemes for (2.1). Up to the imaginary unit, A and B will stand for the kinetic and potential operators below, as in Equation (1.1), for example. Exponential

☆ The review of this paper was arranged by Prof. Blum Volker.

E-mail address: evgueni.dinvay@uit.no.

https://doi.org/10.1016/j.cpc.2024.109438

Available online 19 November 2024

integrators form a significant class of splitting methods [4,14] for the numerical integration of differential equations of the form (2.1). The applicability of these schemes for nonlinear Schrödinger type equations is supported by simulations conducted in [22], for example, see also the references therein.

2.1. Time independent potential

Let A, B be constant. Then the propagator $\mathscr{T}$ reduces to the one-parameter family $\mathscr{T}(t_2,t_1)=\mathscr{T}(t_2-t_1)$ with $\mathscr{T}(t)=e^{(A+B)t}$ called a semigroup. In general the operators A and B do not commute, and so this expression cannot be simplified as the multiplication of the two semigroups associated with A and B. However, such a substitution is valid to first order for small values of t, namely,

$$e^{At+Bt}=e^{At}e^{Bt}+\mathscr{O}(t^2). \tag{2.2}$$

A subsequent application of the multiplication $e^{At}e^{Bt}$ to a given initial data $u(0)$ would provide us with the solution at a given final time moment with first order $\mathscr{O}(t)$ of accuracy. A more accurate result one can get with the symmetric symplectic scheme (1.3). General higher order factorisations of this type were systematically investigated in [19,26]. For any given positive integer n one can decompose the semigroup $\mathscr{T}(t)$ as

$$e^{At+Bt}=e^{At_1}e^{Bt_2}e^{At_3}e^{Bt_4}\dots e^{At_M}+\mathscr{O}(t^{n+1}) \tag{2.3}$$

with some appropriately chosen parameters $t_1,\dots,t_M$. This allows to set larger time steps and accelerate computations. However, it turns out that number of terms M increases exponentially with the order of the approximation n. In practical applications, the integrator order n does not usually exceed 8, because the number of terms in (2.3) outweighs the benefits of a larger time step.

The time parameters $t_1,\dots,t_M$ are not unique. Below we pay special attention to those factorisations that contain the biggest possible absolute values $|t_j|$, which in turn maximises the sparsity of the multiwavelet (MW) representation of the operators $\exp\left(it_j\partial_x^2\right)$ in the decomposition (2.3).

So far we have not employed the fact that A and B stand for the kinetic and potential energy operators, respectively. An advantage of this particular choice was taken in [6,8,21], where several fourth order schemes were introduced allowing minimal amount of exponents in the decomposition (2.3). Among them, we extensively use the following decomposition

$$e^{At+Bt}=\exp\left(\frac{t}{6}B\right)\exp\left(\frac{t}{2}A\right)\exp\left(\frac{2t}{3}\widetilde{B}\right)\exp\left(\frac{t}{2}A\right)\exp\left(\frac{t}{6}B\right)+\mathscr{O}(t^5), \tag{2.4}$$

where

$$\widetilde{B}=\widetilde{B}(t)=B+\frac{t^2}{48}[B,[A,B]].$$

This double commutator is proportional to the squared gradient of the potential $(\partial_x V)^2$, which makes $\widetilde{B}$ a potential operator when $B=-iV$. Indeed,

$$\widetilde{B}=-i\widetilde{V},\quad \widetilde{V}=\begin{cases} V-\dfrac{t^2}{24}(\partial_x V)^2, & A=i\partial_x^2, \quad B=-iV \\ V-\dfrac{t^2}{48}(\partial_x V)^2, & A=\dfrac{i}{2}\partial_x^2, \quad B=-iV \end{cases}, \tag{2.5}$$

where we regarded two of the most used normalisations for the kinetic energy operator. The fourth order scheme (2.4) requires only two applications of the free-particle semigroup operator. On the contrary one needs to know the gradient of the potential. For comparison we mention an alternative scheme from [8] reading

$$e^{At+Bt}=\exp\left(\frac{t}{8}\widetilde{B}\right)\exp\left(\frac{t}{3}A\right)\exp\left(\frac{3t}{8}B\right)\exp\left(\frac{t}{3}A\right)\exp\left(\frac{3t}{8}B\right)\exp\left(\frac{t}{3}A\right)\exp\left(\frac{t}{8}\widetilde{B}\right)+\mathscr{O}(t^5), \tag{2.6}$$

where $\widetilde{B}$ is again defined in (2.5). In the latter scheme, the free-particle operator $\exp\left(\frac{t}{3}A\right)$ appears 3 times instead of two, and the factor $1/3$ in front of tA makes its multiresolution less sparse compared to $\exp\left(\frac{t}{2}A\right)$ standing in (2.4). Scheme (2.6) could however be used alongside (2.4) for precision control. The operator splitting (2.4) is far superior to any other existing fourth order symplectic algorithm, to our knowledge.

These algorithms can be recursively extended to higher order schemes [8]. Denoting by $\mathscr{T}$ the evolution operator $\mathscr{T}(t)=e^{At+Bt}$ and by $\mathscr{T}^{(n)}$ its n-th order approximation, that is $\mathscr{T}(t)=\mathscr{T}^{(n)}(t)+\mathscr{O}\left(t^{n+1}\right)$, we can express an $n+2$ order scheme as

$$\mathscr{T}^{(n+2)}(t)=\mathscr{T}^{(n)}(t_n)\mathscr{T}^{(n)}(-s_nt_n)\mathscr{T}^{(n)}(t_n),\quad t_n=\frac{t}{2-s_n},\quad s_n=2^{1/(n+1)}. \tag{2.7}$$

A proof can be found in [26]. A few remarks can be made concerning this recursive formula:

(1) $\mathscr{T}(-t)=\mathscr{T}^{-1}(t)$ that is in connection to the Schrödinger equation coincides with the adjoint $\mathscr{T}^*(t)$;
(2) $s_nt_n>t_n>t$, which provides us with a little advantage of exploiting (2.7), since both precision and sparsity of the free particle propagator multiresolution increase together with the time step size;
(3) there is an obvious drawback behind (2.7), as the amount of work is increasing three times per time step whenever one goes for a higher order scheme.

As a working example of a sixth order scheme, we iterate $\mathscr{T}^{(4)}$ given by (2.4) using (2.7) to get

$$\begin{aligned}\mathscr{T}^{(6)}(t)=&\exp\left(\frac{t_4}{6}B\right)\exp\left(\frac{t_4}{2}A\right)\exp\left(\frac{2t_4}{3}\widetilde{B}(t_4)\right)\exp\left(\frac{t_4}{2}A\right)\exp\left(\frac{(1-s_4)t_4}{6}B\right)\exp\left(-\frac{s_4t_4}{2}A\right)\exp\left(-\frac{2s_4t_4}{3}\widetilde{B}(s_4t_4)\right)\\&\exp\left(-\frac{s_4t_4}{2}A\right)\exp\left(\frac{(1-s_4)t_4}{6}B\right)\exp\left(\frac{t_4}{2}A\right)\exp\left(\frac{2t_4}{3}\widetilde{B}(t_4)\right)\exp\left(\frac{t_4}{2}A\right)\exp\left(\frac{t_4}{6}B\right).\end{aligned} \tag{2.8}$$

Here the last 6 operators are identical to the first 6 ones in reverse order, so that the whole operator $\mathscr{T}^{(6)}(t)$ is symmetric. Note that this scheme demands 6 applications of kinetic energy exponent per time step. If we continue the recursive procedure (2.7) we will arrive to an eighth order scheme demanding 18 applications, correspondingly. Although it is still

a reasonable amount, there is a slightly better alternative derived by Yoshida [26] that we describe next. It is clear from the iterative procedure (2.7) that an even order symmetric integrator can have the form

$$\mathscr{T}^{(n)}(t)=\mathscr{T}^{(2)}(w_m t)\ldots\mathscr{T}^{(2)}(w_0 t)\ldots\mathscr{T}^{(2)}(w_m t)$$

with $2m+1$ second order integrators $\mathscr{T}^{(2)}(t)$ defined by the splitting (1.3) and some weights $w_0, w_1, \ldots, w_m$. Number m and these weights depend on the order n. However, a direct implementation of (2.7) does not necessarily give the most optimal representation. It turns out that m can be brought down to $m=3$ for the order $n=6$ and to $m=7$ for the order $n=8$. The choice of weights w_j is not unique, and we select those providing us with the largest value of $\min\limits_{j=0,\ldots,m}|w_j|$. Their values are reported in Table 1.

Thus both 6th and 8th order Yoshida integrators can be combined together in the product

$$\mathscr{T}^{(n)}(t)=\exp\,(c_1 tB)\exp\,(d_1 tA)\exp\,(c_2 tB)\cdot\ldots\cdot\exp\,(d_{2m+1}tA)\exp\,(c_{2m+2}tB) \tag{2.9}$$

where t is the time step and c_i, d_i are constants given by

$$c_1=c_{2m+2}=\frac{w_m}{2},\quad c_2=c_{2m+1}=\frac{w_m+w_{m-1}}{2},\quad \ldots \\ ,c_{m+1}=c_{m+2}=\frac{w_1+w_0}{2}$$

and

$$d_1=d_{2m+1}=w_m,\quad d_2=d_{2m}=w_{m-1},\quad \ldots,\quad d_m=d_{m+2}=w_1 \\ ,d_{m+1}=w_0.$$

The integrator is symmetric. Moreover, it is quite general, as it does not require the knowledge of the potential gradient $\partial_x V(x)$. The 8th order scheme demands 15 kinetic exponent applications, less than the 18 corresponding to the twice-iterated (2.4) by (2.7). The weights associated with the latter lie in the interval $[0.65, 0.84]$ in absolute value, as one can easily deduce from (2.4), (2.7). Thus in the case of stationary potential $V(x)$ one may anticipate the best performance for a given order as follows:

order $n=4$: Scheme (2.4)
order $n=6$: Scheme (2.8)
order $n=8$: Scheme (2.9)

Although the difference between Scheme (2.8) and Scheme (2.9) may seem minor for the case $n=6$, in [8] it is claimed that (2.8) outperforms slightly (2.9), at least for the scattering experiment regarded there. We confirm their conclusion below on a different numerical experiment.

2.2. Time dependent potential

Now let $B=B(t)$, the propagator $\mathscr{T}=\mathscr{T}(t+\tau,t)$ can still be approximated at a small time step $\tau=\Delta t$ by exponential operators. An n-th order integrator propagating solutions of (2.1) through the interval $[t,t+\tau]$ are denoted by $\mathscr{T}^{(n)}(t+\tau,t)$, meaning $\mathscr{T}(t+\tau,t)=\mathscr{T}^{(n)}(t+\tau,t)+\mathscr{O}(\tau^{n+1})$. Using Suzuki's formal approach [20] we extend the schemes from the previous subsection to the current situation. Let $\mathscr{D}$ be the forward time derivative operator, called also the super-operator in [20], that is a time derivative acting on functions standing on the left, namely,

$$F(t)e^{\tau\mathscr{D}}G(t)=F(t+\tau)G(t) \tag{2.10}$$

for any time-dependent functions $F(t)$ and $G(t)$. In particular, $e^{\tau\mathscr{D}}G(t)=G(t)$. With the help of this super-operator the propagator is reduced to the exponential representation

$$\mathscr{T}(t+\tau,t)=\exp\,(\tau(A+B(t)+\mathscr{D})). \tag{2.11}$$

Combining A and $\mathscr{D}$ together, then approximating this exponent exactly as was done in the previous subsection with $A+\mathscr{D}$ standing now in place of A, we can extend all the above schemes. Note that A does not depend on time, so A and $\mathscr{D}$ commute. Therefore, $\exp\,(\tau(A+\mathscr{D}))=\exp\,(\tau A))\exp\,(\tau\mathscr{D})$. Thus approximating the exponent in (2.11) by the second order scheme (1.3) one deduces

$$\mathscr{T}(t+\tau,t)=\exp\left(\frac{\tau}{2}B(t)\right)\exp\,(\tau(A+\mathscr{D}))\exp\left(\frac{\tau}{2}B(t)\right)+\mathscr{O}(t^3)$$

which together with the super-operator property (2.10) leads to the following simple second order splitting

$$\mathscr{T}^{(2)}(t+\tau,t)=\exp\left(\frac{\tau}{2}B(t+\tau)\right)\exp\,(\tau A)\exp\left(\frac{\tau}{2}B(t)\right). \tag{2.12}$$

In the same manner we extend both 6th and 8th order Yoshida integrators to

$$\mathscr{T}^{(n)}(t+\tau,t)=\exp\,(c_1\tau B(t+b_1\tau))\exp\,(d_1\tau A)\exp\,(c_2\tau B(t+b_2\tau)) \\ \cdot\ldots\cdot\exp\,(d_{2m+1}\tau A)\exp\,(c_{2m+2}\tau B(t+b_{2m+2}\tau)), \tag{2.13}$$

where b_k are constants given by

$$b_k=\sum_{j=k}^{2m+1}d_j=1-\sum_{j=1}^{k-1}d_j,$$

in particular, $b_1=1$ and $b_{2m+2}=0$.

A scheme for time dependent potentials analogous to (2.4), that is also provided in [9], reads

$$\mathscr{T}^{(4)}(t+\tau,t)=\exp\left(\frac{\tau}{6}B(t+\tau)\right)\exp\left(\frac{\tau}{2}A\right)\exp\left(\frac{2\tau}{3}\widetilde{B}\left(t+\frac{\tau}{2},\tau\right)\right)\exp\left(\frac{\tau}{2}A\right)\exp\left(\frac{\tau}{6}B(t)\right), \tag{2.14}$$

where the modified potential evaluated at the central time step moment is defined as

$$\widetilde{B}(t,\tau)=B(t)+\frac{\tau^2}{48}[B(t),[A,B(t)]]. \tag{2.15}$$

This follows from (2.11), (2.4), (2.10) and the identity $[B(t),[\mathscr{D},B(t)]]=0$. The latter can be checked directly

$$F(t)[B(t),[\mathscr{D},B(t)]]=2F(t)B(t)\mathscr{D}B(t)-F(t)B^2(t)\mathscr{D}-F(t)\mathscr{D}B^2(t)=0$$

on any smooth test operator $F(t)$. Scheme (2.14) is very useful, since the commutator in (2.15) turns out to be proportional to $\partial_x V(x,t)$ for the Schrödinger equation. It is worth to mention that this scheme was recently extended to the Dirac equation [25]. Similarly, the sixth order integrator (2.8) turns into

Table 1
The weights for the selected integrators for order $n=6$ and $n=8$. The numerical values correspond to set A from Table 1 and set C from Table 2 in [26].

	$n=6$	$n=8$
w_0	1.315186320683906	1.65899088454396
w_1	-1.17767998417887	0.311790812418427
w_2	0.235573213359357	-1.55946803821447
w_3	0.784513610477560	-1.67896928259640
w_4		1.66335809963315
w_5		-1.06458714789183
w_6		1.36934946416871
w_7		0.629030650210433

$$\begin{aligned}\mathscr{T}^{(6)}(t+\tau,t)=&\exp\left(\frac{\tau_4}{6}B(t+(2-s_4)\tau_4)\right)\exp\left(\frac{\tau_4}{2}A\right)\\&\cdot\exp\left(\frac{2\tau_4}{3}\widetilde{B}\left(t+\left(\frac{3}{2}-s_4\right)\tau_4,\tau_4\right)\right)\\&\cdot\exp\left(\frac{\tau_4}{2}A\right)\exp\left(\frac{(1-s_4)\tau_4}{6}B(t+(1-s_4)\tau_4)\right)\exp\left(-\frac{s_4\tau_4}{2}A\right)\\&\cdot\exp\left(-\frac{2s_4\tau_4}{3}\widetilde{B}\left(t+\left(1-\frac{s_4}{2}\right)\tau_4,s_4\tau_4\right)\right)\exp\left(-\frac{s_4\tau_4}{2}A\right)\\&\cdot\exp\left(\frac{(1-s_4)\tau_4}{6}B(t+\tau_4)\right)\\&\cdot\exp\left(\frac{\tau_4}{2}A\right)\exp\left(\frac{2\tau_4}{3}\widetilde{B}\left(t+\frac{\tau_4}{2},\tau_4\right)\right)\exp\left(\frac{\tau_4}{2}A\right)\exp\left(\frac{\tau_4}{6}B(t)\right).\end{aligned}\tag{2.16}$$

Note that we first extended the time-independent potential scheme (2.4) to (2.8) via recursion (2.7). Afterwards we applied the Suzuki decomposition method (2.11) to deduce (2.16) from (2.8). Integrator (2.14) can also be directly extended to higher order schemes by the general Suzuki's recursive procedure

$$\begin{aligned}\mathscr{T}^{(n+2)}(t+\tau,t)=&\mathscr{T}^{(n)}(t+\tau,t+(1-\kappa_n)\tau)\mathscr{T}^{(n)}(t+(1-\kappa_n)\tau,t+(1-2\kappa_n)\tau)\\&\cdot\mathscr{T}^{(n)}(t+(1-2\kappa_n)\tau,t+2\kappa_n\tau)\mathscr{T}^{(n)}(t+2\kappa_n\tau,t+\kappa_n\tau)\mathscr{T}^{(n)}(t+\kappa_n\tau,t)\end{aligned}\tag{2.17}$$

with $\kappa_n=\left(4-4^{1/(n+1)}\right)^{-1}$, as mentioned in [24]. However, this procedure leads rapidly to expensive integrators: for instance, the 8-th order scheme demands 50 applications of the kinetic energy exponents per time step. Therefore, we implemented it only to derive $\mathscr{T}^{(6)}$ from $\mathscr{T}^{(4)}$ given in (2.14). The corresponding integrator reads

$$\begin{aligned}\mathscr{T}^{(6)}(t+\tau,t)=&\exp\left(\frac{\kappa_4\tau}{6}B(t+\tau)\right)\exp\left(\frac{\kappa_4\tau}{2}A\right)\\&\cdot\exp\left(\frac{2\kappa_4\tau}{3}\widetilde{B}\left(t+\left(1-\frac{\kappa_4}{2}\right)\tau,\kappa_4\tau\right)\right)\\&\cdot\exp\left(\frac{\kappa_4\tau}{2}A\right)\exp\left(\frac{\kappa_4\tau}{3}B(t+(1-\kappa_4)\tau)\right)\exp\left(\frac{\kappa_4\tau}{2}A\right)\\&\cdot\exp\left(\frac{2\kappa_4\tau}{3}\widetilde{B}\left(t+\left(1-\frac{3}{2}\kappa_4\right)\tau,\kappa_4\tau\right)\right)\\&\cdot\exp\left(\frac{\kappa_4\tau}{2}A\right)\exp\left(\frac{(1-3\kappa_4)\tau}{6}B(t+(1-2\kappa_4)\tau)\right)\exp\left(\frac{(1-4\kappa_4)\tau}{2}A\right)\\&\cdot\exp\left(\frac{2(1-4\kappa_4)\tau}{3}\widetilde{B}\left(t+\frac{\tau}{2},(1-4\kappa_4)\tau\right)\right)\exp\left(\frac{(1-4\kappa_4)\tau}{2}A\right)\\&\cdot\exp\left(\frac{(1-3\kappa_4)\tau}{6}B(t+2\kappa_4\tau)\right)\\&\cdot\exp\left(\frac{\kappa_4\tau}{2}A\right)\exp\left(\frac{2\kappa_4\tau}{3}\widetilde{B}\left(t+\frac{3\kappa_4\tau}{2},\kappa_4\tau\right)\right)\exp\left(\frac{\kappa_4\tau}{2}A\right)\\&\cdot\exp\left(\frac{\kappa_4\tau}{3}B(t+\kappa_4\tau)\right)\exp\left(\frac{\kappa_4\tau}{2}A\right)\\&\cdot\exp\left(\frac{2\kappa_4\tau}{3}\widetilde{B}\left(t+\frac{\kappa_4\tau}{2},\kappa_4\tau\right)\right)\exp\left(\frac{\kappa_4\tau}{2}A\right)\exp\left(\frac{\kappa_4\tau}{6}B(t)\right)\end{aligned}\tag{2.18}$$

with positive $\kappa_4\approx0.4$ and negative $1-4\kappa_4\approx-0.5$ weights in front of kinetic operator. These weights together with the large number of applications of the kinetic energy exponentials, make (2.18) less convenient to use compared to (2.16), though it may give better results for some time steps.

We would like to conclude this section with some discussion on causality. One can notice that several schemes presented above include negative time steps that is definitely satisfactory from a mathematical order analysis perspective. As a matter of fact, beyond second order $n>2$, every factorisation of the form (2.3) must necessarily contain at least one negative parameter among $t_1,\dots,t_M$. This was essentially proved by Sheng [17] and later refined by Suzuki [18]. It was then precised and extended even more in [12]. Note that Scheme (2.4) represents a different factorisation from (2.3), since it contains an additional operator $\widetilde{B}$, and it therefore constitutes an exception. Both (2.4) and its non-autonomous counterpart (2.14) contain only positive time steps. From a numerical stability perspective it is not a problem, unless one needs to perform quantum statistical calculations [7]. Though in [6,8] it is observed that the general integrators (2.3) of the fourth order with negative times are less precise than the time-positive gradient schemes (2.4), (2.6). In other words, the simulations provided in [6,8] may suggest that one needs smaller time steps in order to achieve the same accuracy, when a scheme with a negative time step is in use, provided, of course, that the methods under comparison are of the same order. On the contrary, we believe that Schemes (2.4), (2.6) outperform the general decomposition (2.3) with $n=4$, because (2.4), (2.6) possess more information about the dynamical system under consideration. In other words, the additional restriction (2.5) might lead to the better performance, whereas the signs of time parameters are irrelevant. Our claim is supported by numerical simulations below, see the explanation accompanying Fig. 4 in Section 3.1.

Finally, we remark that it may seem that negative time steps break causality. However, one may notice that all the time moments, at which we evaluate potentials V and $\widetilde{V}$, in all the schemes given above, are actually positive. In other words, the wave dynamics of (2.1) is completely defined by an initial data $u(0)$, and one does not have to consider solutions at negative time moments, even though the time steps in the integrators in use may be negative. In fact, the obligatory presence of negative time steps in the high order schemes has a simple physical explanation. Indeed, a wave corresponding to the free-particle disperses with time. The only way to localise the wave is to impose a certain potential. High order schemes allow the use of bigger time steps. However, it should be clear that due to the serious dispersion at a longer time period, the potential may not be strong enough to localise the wave back into space. So the focusing happens partially due to the inverse kinetic exponential operator, namely, the free-particle semigroup with a negative time parameter, necessarily standing in the factorisation (2.3).

3. Numerical experiments

The free-particle semigroup $\exp\left(it\partial_x^2\right)$ is encoded in `MRCPP` (Multiresolution Computation Program Package) [1]. `MRCPP` is a high-performance C++ library, which provides various tools for working with Multiwavelets in connection to computational chemistry. It is also made available in `VAMPyR` (Very Accurate Multiwavelets Python Routines) [2], which builds on the `MRCPP` capabilities, providing an easy to use interface. As an introduction to this software, we refer to our recent article [3], where we have already included a simple numerical experiment with the exponential operator $\exp\left(it\partial_x^2\right)$. In [3], we did not exploit the sparsity analysed thoroughly in the first part of the current

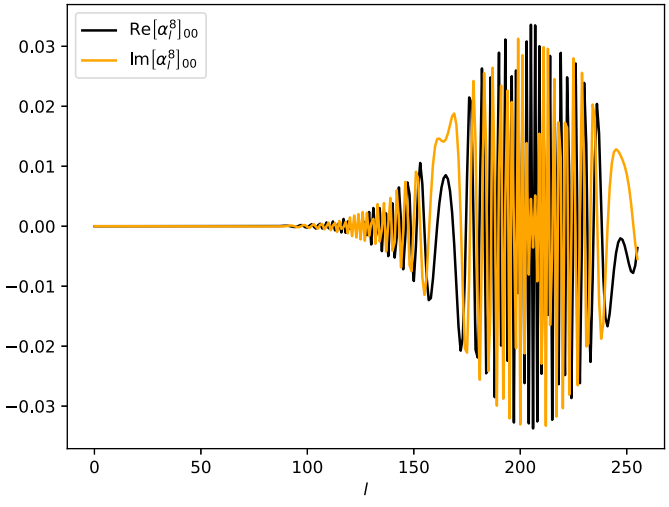

Fig. 1. Matrix element $\left[\alpha_l^n\right]_{pj}$ with $p=j=0$ at scale $n=8$ corresponding to the time step $t=0.0001$ and the MRA order $\mathbb{k}=6$.

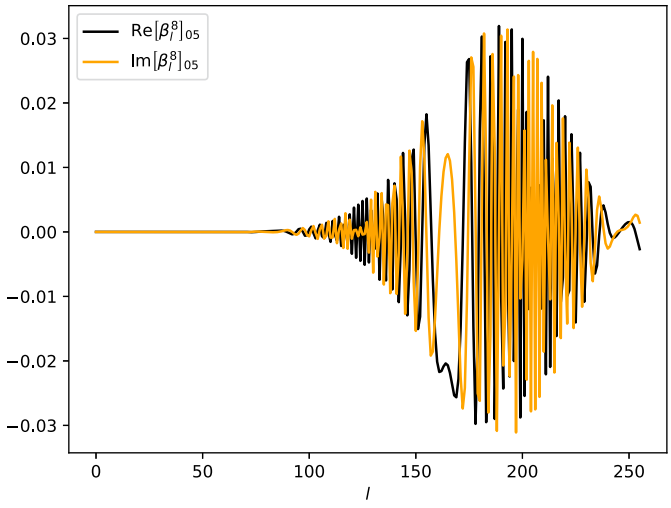

Fig. 2. Matrix element $[\beta_l^n]_{pj}$ with $p=0$, $j=5$ at scale $n=8$ corresponding to the time step $t=0.0001$ and the MRA order $\mathbb{f}=6$.

contribution [11]. In order to construct the adaptive multiresolution representation of $\exp\left(it\partial_x^2\right)$, the threshold is set to $\varepsilon/10$ for a given precision ε. In other words, the matrices α_l^n, β_l^n, γ_l^n having the Frobenius norm less or equal than $\varepsilon/10$, are ignored in numerical calculations. This choice of threshold is motivated by oscillatory behaviour of the matrix entries $[\alpha_l^n]_{pj}$, $[\beta_l^n]_{pj}$, $[\gamma_l^n]_{pj}$ with respect to the distance to diagonal l, on the one hand, see Figs. 1, 2 and compare with figures for the corresponding norms given in the first part of this paper [11]. On the other hand, the result of operator application was controlled by the free-particle analytical solution to (1.2) of the form

$$u(x,t)=\exp\left(it\partial_x^2\right)\psi_0(x)=\left(\frac{1}{2\pi\sigma^2}\right)^{1/4}\sqrt{\frac{4\sigma^2}{4it+4\sigma^2}}e^{-\frac{(x-x_0)^2}{4it+4\sigma^2}} \tag{3.1}$$

associated with the initial condition

$$\psi_0(x)=\left(\frac{1}{2\pi\sigma^2}\right)^{1/4}\exp\left(-\frac{(x-x_0)^2}{4\sigma^2}\right) \tag{3.2}$$

in the sense $u(x,0)=\psi_0(x)$. Indeed, let $x_0=0.5$ and $\sigma=0.04$, for example. Then for the MRA order $\mathbb{f}=20$, time parameter $t=0.0001$ and precision $\varepsilon=10^{-10}$ the L^2-norm of the difference between analytical and numerically propagated solutions is $2.0\cdot10^{-11}$, see Fig. 3.

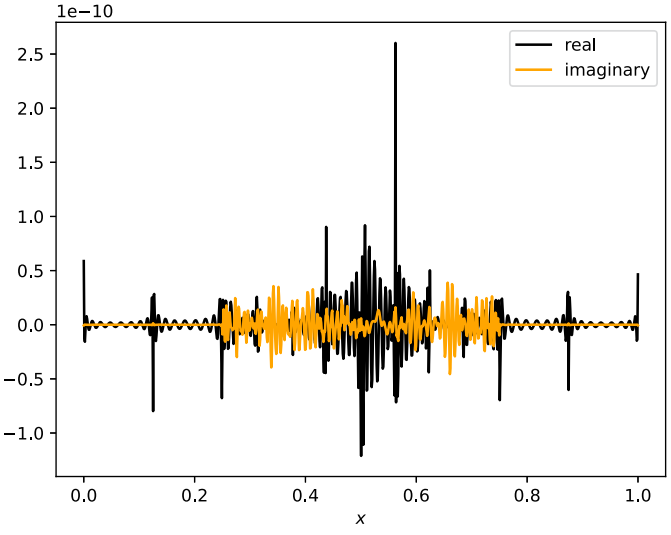

Fig. 3. Difference between the analytical solution (3.1) and the numerically propagated one at the time moment $t=0.0001$ for the MRA order $\mathbb{f}=20$ and the precision $\varepsilon=10^{-10}$.

This concludes the description of the numerical implementation of the free-particle propagator. Below we illustrate its use on two toy model problems and we compare its performance to the periodic spectral method.

3.1. Harmonic potential

Our first numerical example takes the Schrödinger equation

$$i\partial_t\psi=-\frac{1}{2}\partial_x^2\psi+V(x)\psi$$

with the harmonic potential

$$V(x)=V_0\left(x-\frac{1}{2}\right)^2.$$

It is complemented by the initial condition $\psi(0)=\psi_0$ having the Gaussian form (3.2). It is well known that in the harmonic potential the density $|\psi(t)|^2$ oscillates with the period $t_{\text{per}}=\pi\sqrt{2/V_0}$, namely, $\psi\left(t_{\text{per}}\right)=-\psi_0$. This comes from the fact that the eigenvalues for the Hamiltonian are $\sqrt{2V_0}(n+1/2)$.

Ideally, a choice of parameters like V_0 should be physically motivated. Then given some tolerance one can set the computational domain of size L centred, for our example, at $x=1/2$. Transforming the problem to the unit space interval $[0,1]$, one will obviously get that the final V_0 turns out to be proportional to L^4. Therefore, we set the following parameters $V_0=98304$, $x_0=0.375$ and $\sigma=0.025$ associated with the domain $[0,1]$.

We conduct numerical simulations with time step τ ranging from $t_{\text{per}}/10$ to $t_{\text{per}}/160$ up to the final time moment $t=t_{\text{per}}$ using the machinery developed here. The integrators in use are referred as follows

(S2) the simple second order scheme (1.3),
(A4) the Chin-Chen's scheme A of fourth order (2.4),
(A6) the Chin-Chen's scheme A of sixth order (2.8),
(Y6) the Yoshida's scheme (2.9) with the order $n=6$,
(Y8) the Yoshida's scheme (2.9) with the order $n=8$.

The accuracy of the obtained solution ψ for each of these schemes is estimated by the L^2-difference

$$\text{error}(t)=\left\|\psi(t)-\psi_{\text{ref}}(t)\right\|_{L^2(0,1)}. \tag{3.3}$$

Here we calculate the error at the moment $t=t_{\text{per}}$ with respect to the reference $\psi_{\text{ref}}\left(t_{\text{per}}\right)=-\psi_0$. For the multiwavelet calculations we take the MRA order $\mathbb{f}=18$ and the tolerance needed for adaptive resolution to be $\varepsilon=10^{-10}$. The performance is compared with the Fourier spectral method calculations using 1024 grid points inside of the unit interval $[0,1]$.

The electron dynamics in the harmonic potential well is smooth and it can be viewed as periodic with very high precision. Therefore, there is no surprise that the spectral method outperforms the multiresolution technique in Fig. 4. The accuracy stagnation for the FFT based schemes reveals itself at four times smaller time steps than the corresponding stagnation for the MRA based schemes, with $\tau=t_{\text{per}}/640\approx2.2\cdot10^{-5}$ compared to $\tau=t_{\text{per}}/160\approx8.9\cdot10^{-5}$ for the integrators (A6), (Y6), (Y8). Otherwise, the precision is consistent and the convergence is optimal for each scheme, as indicated by the slopes of curves in Fig. 4 corresponding to their theoretical counterparts. It is also interesting to notice that (Y8) does not reach the accuracy of the cheaper scheme (A6) in the current setup. Moreover, the lines (A6) and (Y6) are parallel, as expected, since they are of the same order. Both splitting methods contain negative

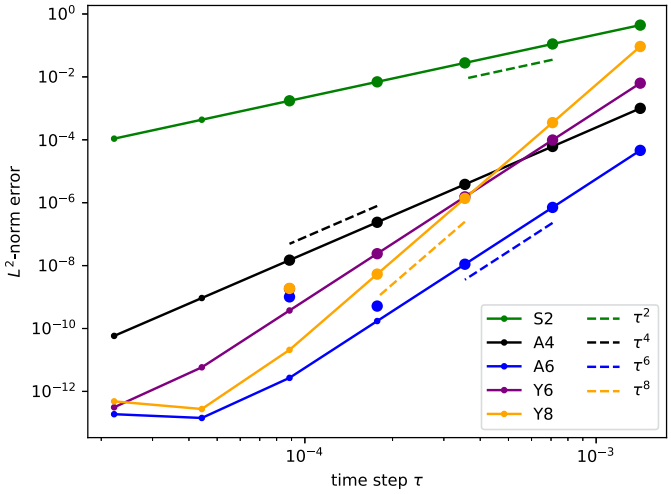

Fig. 4. Convergence comparison between FFT-based schemes (solid lines) and MRA-based schemes (large dots) in the harmonic potential example. The convergence rates are indicated by the dashed lines. The legend corresponds to different integrators: (S2) for (1.3), (A4) for (2.4), (A6) for (2.8), (Y6) for (2.9) with $n=6$ and (Y8) for (2.9) with $n=8$. (For interpretation of the colours in the figure(s), the reader is referred to the web version of this article.)

times. However, (A6) lies significantly lower than (Y6). This is probably due to the fact that (A6) is more specialised towards Schrödinger type equations by the additional relation (2.5), constraining the double commutator standing in $\widetilde{B}$.

3.2. Walker-Preston model

As a prototype of time dependent Hamiltonian, we consider the Walker-Preston model [23] for the vibration of a diatomic molecule in a strong laser field. The equation reads

$$i\partial_t\psi = -\frac{1}{2}\partial_x^2\psi + V(x)\psi + \mathscr{E}(x,t)\psi,$$

where $V(x)$ stands for the Morse potential

$$V(x) = V_0(1-e^{-\alpha x})^2$$

with $V_0 = 0.2251\mu$, $\mu = 1745$ and $\alpha = 1.1741$. These parameters correspond to a model of the HF molecule. Here $\mathscr{E}(x,t) = Ax\cos\omega t$ is the external field with $A = 0.011025\mu$ and $\omega = 0.01787\mu$. The first 0→1 vibrational frequency difference in the Morse oscillator is 0.01807μ, so ω is slightly below resonance. As the initial condition $\psi(0) = \psi_0$ we consider the ground state wave function

$$\psi_0(x) = \sqrt{\alpha\frac{\xi^{2\lambda-1}(x)}{\Gamma(2\lambda-1)}e^{-\xi(x)}}, \quad \xi(x) = 2\lambda e^{-\alpha x}, \quad \lambda = \frac{\sqrt{2V_0}}{\alpha}$$

having the ground state energy

$$E_0 = \alpha\sqrt{\frac{V_0}{2}} - \frac{\alpha^2}{8}.$$

A direct evaluation of $\psi_0(x)$ may lead to large round up errors. Therefore, we rewrite it in a form which is more suitable for numerical calculations. There is an integer $m\in\mathbb{N}$ such that $2\lambda - 1 = m + \delta\lambda$ with $1/2\leqslant\delta\lambda < 3/2$. We can factorise ψ_0 as

$$\psi_0(x) = \sqrt{\alpha\frac{\xi^{\delta\lambda}}{\Gamma(\delta\lambda)}\frac{\xi e^{-\xi/m}}{\delta\lambda}\frac{\xi e^{-\xi/m}}{\delta\lambda+1}\cdots\frac{\xi e^{-\xi/m}}{\delta\lambda+m-1}},$$

thus eliminating the possibility of rounding errors.

All the introduced parameters are associated with the computational domain $[-0.8, 4.32]$ of length $L = 5.12$, which has been used by several authors [5,9,13,15,16] for testing different numerical methods. It is therefore well known that a use of the spectral periodic treatment for this problem with 64 grid points gives very accurate results, making it the ideal benchmark for our purposes. However, our multiresolution technique is working in the computational domain $[0,1]$ and we need to adapt the domain with an affine transformation. Henceforth $x\in[0,1]$ and the time scales $t = t^{\text{original}}/L^2$. All the other units are changed accordingly: for example, the dissociation energy $V_0 = V_0^{\text{original}}L^2 = 0.2251\mu L^2$.

Spectral FFT-based simulations are conducted with a time step τ ranging from 0.001 to $0.001\cdot 2^{-10}$. The final time moment is set to $t_{\text{fin}} = 0.1$. The integrators in use are referred to as follows

(S2) the simple second order scheme (2.12),
(A4) the Chin-Chen's scheme A of fourth order (2.14),
(A6) the Chin-Chen's scheme A of sixth order (2.16),
(W6) the Chin-Chen's scheme A of sixth order (2.18) obtained via the procedure (2.17),
(Y6) the Yoshida's scheme (2.13) with the order $n = 6$,
(Y8) the Yoshida's scheme (2.13) with the order $n = 8$.

The accuracy of the obtained solution ψ for each of these schemes is estimated by (3.3) at the final time moment $t = t_{\text{fin}}$. Contrary to the previous example, we do not have an analytical result that could stand in place of ψ_{ref} as in the previous experiment. Presuming we do not know *a priori* which scheme is the most precise, for each scheme we take the result obtained with the smallest time step as the corresponding reference. For example, ψ_{ref} for the (S2) numerical solutions is the (S2) FFT-based result associated with the time step $\tau = 0.001\cdot 2^{-10}$. The same references are used later on in order to estimate the accuracy of the corresponding multiwavelet simulations.

In fact, we can again see an obvious accuracy outperformance of the periodic spectral method in Fig. 5. This time, however, we knew *a priori* that the best FFT calculations are achieved with the rough grid consisting of only 64 points. Indeed, with a finer grid of 256 or 1024 points, one encounters poorer accuracy due to the Gibbs phenomenon, which causes high oscillations of the numerical solutions close to the boundary of the computational domain. The Gibbs phenomenon does not affect the multiresolution approach, of course. We do not include figures

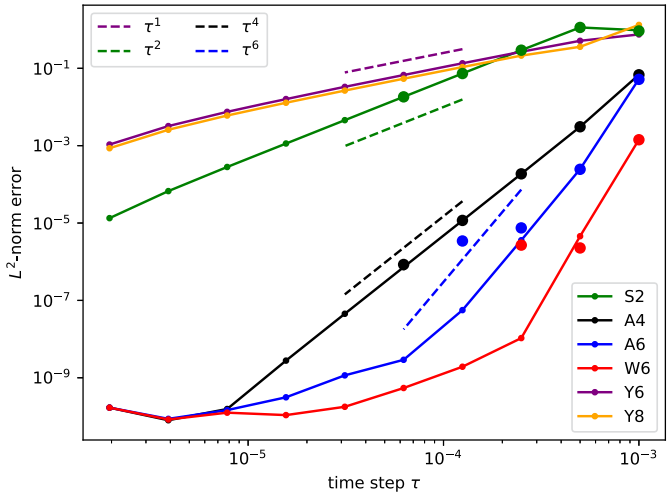

Fig. 5. Convergence comparison between FFT-based schemes (solid lines) and MRA-based schemes (large dots) in the Morse potential example. The convergence rates are indicated by the dashed lines. The legend corresponds to different integrators: (S2) for (2.12), (A4) for (2.14), (A6) for (2.16), (W6) for (2.18), (Y6) for (2.13) with $n=6$ and (Y8) for (2.13) with $n=8$.

corresponding to refined grid FFT calculations here, as they exhibit behaviour similar to Fig. 5. However, these FFT results demonstrate poorer convergence, deviating from the theoretically predicted rate, before the MRA calculations approach stagnation. In other words, FFT-based spectral calculations can yield inferior results compared to MRA-based ones in terms of accuracy.

An interesting and noteworthy outcome is that the extensions (2.13) of Yoshida's schemes (2.9) for the time-dependent potential case degenerate to first order, see Fig. 5. According to [24] it may happen that some exponential integrators lose their theoretically predicted accuracy after the Suzuki's extension described in Subsection 2.2. It seems that Yoshida's schemes (2.9) cannot be efficiently extended to non-autonomous equations. The author encountered a similar problem before [10].

4. Conclusion

We have developed a multiresolution analysis of the semigroup $\exp\left(it\partial_x^2\right)$ and introduced MRA-based numerical methods for solving the time-dependent Schrödinger equation. These methods offer several notable advantages. First of all, they can be seamlessly integrated with existing tools for solving stationary problems. Specifically, the application of singular integral operators arising from the potential V, as utilised in Kohn-Sham and Hartree-Fock theories, is already well-established in multiwavelet bases. Consequently, these techniques can be readily adapted to address time evolution problems. Moreover, these methods offer spatial adaptivity, which is crucial for quantum chemistry simulations. In these simulations, it is essential to handle Coulomb-type singularities and solutions with cusps. Therefore, an automatic grid refinement based on a predefined, arbitrary precision is an advantage.

However, there are some drawbacks to consider. For computational efficiency, it is essential to achieve sparsity in the multiresolution representation of $\exp\left(it\partial_x^2\right)$. This in turn requires large time steps t and a high MRA order $\mathbb{f}$. However, a large polynomial order $\mathbb{f}$ can slow down simulations, while overly large time steps t may compromise the accuracy of the results obtained. The extent to which these issues limit the applicability of the method proposed here, will have to be thoroughly investigated.

One strategy to overcome these challenges, which we plan to focus on soon, is to develop artificial boundary conditions for the MRA-based methods introduced here. This approach will enable us to use larger time steps while maintaining accuracy, by confining the computational domain to a relatively compact size. Additionally, it will also make it possible to use lower $\mathbb{f}$ values, boosting efficiency. The techniques developed will be applied to problems where FFT-based methods encounter challenges, specifically in modelling the attosecond dynamics of electrons in molecules exposed to intense laser pulses.

Declaration of Competing Interest

The authors declare the following financial interests/personal relationships which may be considered as potential competing interests:

Luca Frediani reports financial support was provided by UiT The Arctic University of Norway. Evgueni Dinvay reports a relationship with UiT The Arctic University of Norway that includes: employment and funding grants. If there are other authors, they declare that they have no known competing financial interests or personal relationships that could have appeared to influence the work reported in this paper.

Acknowledgements

The author is grateful to S. R. Jensen and Ch. Tantardini for numerous helpful discussions. I acknowledge support from the Research Council of Norway through its Centres of Excellence scheme (Hylleraas centre, 262695). Special thanks to my supervisor L. Frediani who introduced me to the problem, read the whole manuscript and supported financially from the Research Council of Norway through the FRIPRO grant ReMRChem (324590), and from NOTUR – The Norwegian Metacenter for Computational Science through grant of computer time (nn14654k). Finally, I would like to thank the anonymous referees, whose valuable comments helped to improve the paper during the revision.

References

[1] Mrcpp repository, 2024. Accessed: 9 February 2024.
[2] Vampyr repository, 2024. Accessed: 9 February 2024.
[3] M. Bjørgve, C. Tantardini, S.R. Jensen, G.A. Gerez, P. Wind, R. Di Remigio Eikås, E. Dinvay, L. Frediani, VAMPyR—a high-level Python library for mathematical operations in a multiwavelet representation, 04.2024.
[4] S. Blanes, F. Casas, A Concise Introduction to Geometric Numerical Integration, Chapman and Hall/CRC, New York, July 2016.
[5] S. Blanes, P. Moan, Splitting methods for the time-dependent Schrödinger equation, Phys. Lett. A 265 (1) (2000) 35–42.
[6] S.A. Chin, Symplectic integrators from composite operator factorizations, Phys. Lett. A 226 (6) (1997) 344–348.
[7] S.A. Chin, Quantum statistical calculations and symplectic corrector algorithms, Phys. Rev. E 69 (Apr. 2004) 046118.
[8] S.A. Chin, C.R. Chen, Fourth order gradient symplectic integrator methods for solving the time-dependent Schrödinger equation, J. Chem. Phys. 114 (17) (05.2001) 7338–7341.
[9] S.A. Chin, C.R. Chen, Gradient symplectic algorithms for solving the Schrödinger equation with time-dependent potentials, J. Chem. Phys. 117 (4) (07.2002) 1409–1415.
[10] E. Dinvay, H. Kalisch, E.I. Părău, Fully dispersive models for moving loads on ice sheets, J. Fluid Mech. 876 (2019) 122–149.
[11] E. Dinvay, Y. Zabelina, L. Frediani, Multiresolution of the one dimensional free-particle propagator. Part 1: Construction, Comput. Phys. Commun. 308 (March 2025) 109436, https://doi.org/10.1016/j.cpc.2024.109436.
[12] D. Goldman, T.J. Kaper, Nth-order operator splitting schemes and nonreversible systems, SIAM J. Numer. Anal. 33 (1) (1996) 349–367.
[13] S.K. Gray, J.M. Verosky, Classical Hamiltonian structures in wave packet dynamics, J. Chem. Phys. 100 (7) (04.1994) 5011–5022.
[14] R.I. McLachlan, G.R.W. Quispel, Splitting methods, Acta Numer. 11 (Jan. 2002) 341–434.
[15] U. Peskin, R. Kosloff, N. Moiseyev, The solution of the time dependent Schrödinger equation by the (t,t') method: the use of global polynomial propagators for time dependent Hamiltonians, J. Chem. Phys. 100 (12) (06.1994) 8849–8855.
[16] J.M. Sanz-Serna, A. Portillo, Classical numerical integrators for wave-packet dynamics, J. Chem. Phys. 104 (6) (02.1996) 2349–2355.
[17] Q. Sheng, Solving linear partial differential equations by exponential splitting, IMA J. Numer. Anal. 9 (2) (04.1989) 199–212.
[18] M. Suzuki, General theory of fractal path integrals with applications to many-body theories and statistical physics, J. Math. Phys. 32 (2) (02.1991) 400–407.
[19] M. Suzuki, General theory of higher-order decomposition of exponential operators and symplectic integrators, Phys. Lett. A 165 (5) (1992) 387–395.
[20] M. Suzuki, General decomposition theory of ordered exponentials, Proc. Jpn. Acad. Ser. B 69 (7) (1993) 161–166.
[21] M. Suzuki, New scheme of hybrid exponential product formulas with applications to quantum Monte-Carlo simulations, in: D.P. Landau, K.K. Mon, H.-B. Schüttler (Eds.), Computer Simulation Studies in Condensed-Matter Physics VIII, Berlin, Heidelberg, Springer Berlin Heidelberg, 1995, pp. 169–174.
[22] M. Thalhammer, M. Caliari, C. Neuhauser, High-order time-splitting Hermite and Fourier spectral methods, J. Comput. Phys. 228 (3) (2009) 822–832.
[23] R.B. Walker, R.K. Preston, Quantum versus classical dynamics in the treatment of multiple photon excitation of the anharmonic oscillator, J. Chem. Phys. 67 (5) (09.1977) 2017–2028.
[24] N. Wiebe, D. Berry, P. Høyer, B.C. Sanders, Higher order decompositions of ordered operator exponentials, J. Phys. A, Math. Theor. 43 (6) (Jan. 2010) 065203.
[25] J. Yin, A fourth-order compact time-splitting method for the Dirac equation with time-dependent potentials, J. Comput. Phys. 430 (2021) 110109.
[26] H. Yoshida, Construction of higher order symplectic integrators, Phys. Lett. A 150 (5) (1990) 262–268.